On the influence of initial guess DEM for gcp-less digital elevation model extraction using photogrammetry on SPOT-6/7 tri-stereo imagery – A case study of South Sulawesi

Zylshal Zylshal[1*], Parwati Sofan[1], Indri Pratiwi J[2], Athar Abdurrahman Bayanuddin[3,4]

[1]Research Center for Geoinformatics, National Research and Innovation Agency (BRIN), Bandung, Indonesia

[2]Bureau for Public Communication, General Affairs, and Secretariat, National Research and Innovation Agency (BRIN), Jakarta, Indonesia

[3]Directorate of Laboratory Management, Research Facilities, and Science and Technology Park, National Research and Innovation Agency (BRIN), Jakarta, Indonesia

[4]Remote Sensing Graduate Study Program, Universitas Gadjah Mada, Indonesia

*zylshal@brin.go.id

Abstract: *Digital Elevation Model (DEM) generation from satellite photogrammetry is a well-established method for extracting topographic information from optical stereo imagery. With the increasing agility of modern satellites, tri-stereo acquisitions (SPOT-6/7, Worldview-3) are now commonly available. Although the use of Ground Control Points (GCPs) is standard for ensuring absolute accuracy, their collection is costly, time-consuming, and labor-intensive. To address these limitations, GCP-less DEM extraction approaches have been developed, relying on Rational Polynomial Coefficients (RPCs) and an initial seed DEM to constrain the object-space geometry. This study evaluates the influence of three different seed DEMs—ALOS World 3D (AW3D30), FABDEM, and the Indonesia-specific DEMNAS—on GCP-less DEM extraction using an iterative bundle adjustment approach on SPOT-6/7 panchromatic tri-stereo imagery. Three test sites in South Sulawesi were selected to represent varied landform and land cover characteristics. All DEMs were converted to an ellipsoidal vertical datum for consistency. A total of 27 DEMs were generated at a 6-meter ground sampling distance (GSD) and evaluated based on visual quality, horizontal alignment, and vertical accuracy. Vertical validation was conducted using 86 independent control points (ICPs) obtained through GNSS field surveys. Most outputs showed good visual fidelity, though some contained voids from cloud cover. Horizontal accuracy remained within one pixel across all outputs. Vertical Root Mean Square Error (RMSE) ranged from 1.18 to 4.79 meters. DEMNAS performed best as an initial seed DEM for GCP-less processing, with mean shift magnitude of 0.42 meters (x-direction) and 0.42 meters (y-direction). It also produced the lowest average vertical error, with RMSE, Mean Absolute Error (MAE), and Normalized Median Absolute Deviation (NMAD) of 4 m, 2.57 m, and 2.14 m, respectively. Given the limited availability of DEMNAS, AW3D30 presents a viable globally available alternative. Further testing with additional seed DEMs is recommended to enhance the generalizability of this GCP-less approach.*

Keywords: DEM, GCP-less, SPOT6, Photogrammetry, FABDEM

Introduction

Digital Elevation Models (DEMs) hold a very important part in terrain analysis, hydrology, hazard assessment, as well as infrastructure planning. Terrain modeling using field

measurements is often met with challenging access, high cost, and labour. Furthermore, in humid tropical regions, persistent cloud cover limits airborne surveys. Optical stereo satellite data provide a practical way to mitigate these challenges with larger coverage and higher temporal.

Generating DEMs using photogrammetry for satellite imagery has been developed since 1986 with the launch of the SPOT-1 satellite (Cooper et al., 1987; Swann et al., 1988). The approach and methods have then evolved, adapting to various radiometric, temporal acquisition, topographic reliefs, and land covers.

Several studies have acknowledged the need for automated DEM extraction using photogrammetry without the need for ground control points (GCPs). To mitigate missing GCPs, researchers are looking for a way to ensure high positional accuracy of the image. The most common approach is to use a reference DEM as a constraint during bundle block adjustment or as a reference for DEM co-registration (Cao et al., 2019; Chen et al., 2018; Gonçalves, 2008). The reference DEM used was varied. Some use SRTM (Afsharnia et al., 2022; Chen et al., 2017, 2018; P. Zhou et al., 2018), DEMs provided by local mapping agency (Neigh et al., 2014; Zheng & Zhang, 2016; Zylshal et al., 2024), ASTER GDEM (Cao et al., 2019), ALOS World DEM 30 meter (AW3D30) (Cao et al., 2019). Recent development saw the utilization of space-borne LiDAR data such as the ICESat and/or ICESat-2 used in a dem bias compensation and/or correction (Lee & Hahn, 2024). We then starte

Despite the operational potential, we identified that one practical question remains under-evaluated; how does the choice of initial-guess DEMs influence the final DEM accuracy? Various freely available DEMs are readily available for both Indonesia and worldwide. These public DEMs have their own characteristics (Carrera-Hernández, 2021). Indonesia-specific DEM Nasional (DEMNAS) combines multiple DEM sources to form an 8-meter GSD of DEM/DSM (BIG, 2018). ALOS World DEM 30-meter (AW3D30) is a global Digital Surface Model (DSM) produced from photogrammetric DEM of ALOS PRISM. Forest and Building removed Copernicus DEM (FABDEM) showcases the latest Global DEM product with its "bare-earth" nature. These DEMs represent different surface representation, where AW3D30 is a DSM, FABDEM is a Digital Terrain Model (DTM), and DEMNAS is in between DSM and DTM (Julzarika & Harintaka, 2019). Using different types of DEMs would give is a more comprehensive insight on the GCP-less DEM extraction approach performance. In this study, the GCP-less DEM extraction workflow developed by Zylshal et al. (2024) used a the tested workflow.

South Sulawesi, in Indonesia, provides a good test bed for our study. The region spans coastal plains, karst topography with medium elevation, as well as steep forested hills. The region was also recently undergone massive infrastructure development (Zylshal et al., 2022). Thus, it prompts for an update of the digital elevation model. Utilizing SPOT-6/7 tri-stereo imagery across three different representative areas (Barru, Maros, and Makassar) enables us to comprehensively assess the seed DEMs over different terrain types. Our study, therefore, aims to evaluate and quantify how initial DEM choices affect a GCP-less DEM extraction workflow for SPOT-6/7 tri-stereo imagery across three humid-tropical terrain in South Sulawesi Province, Indonesia.

Methodology

a. Study Area

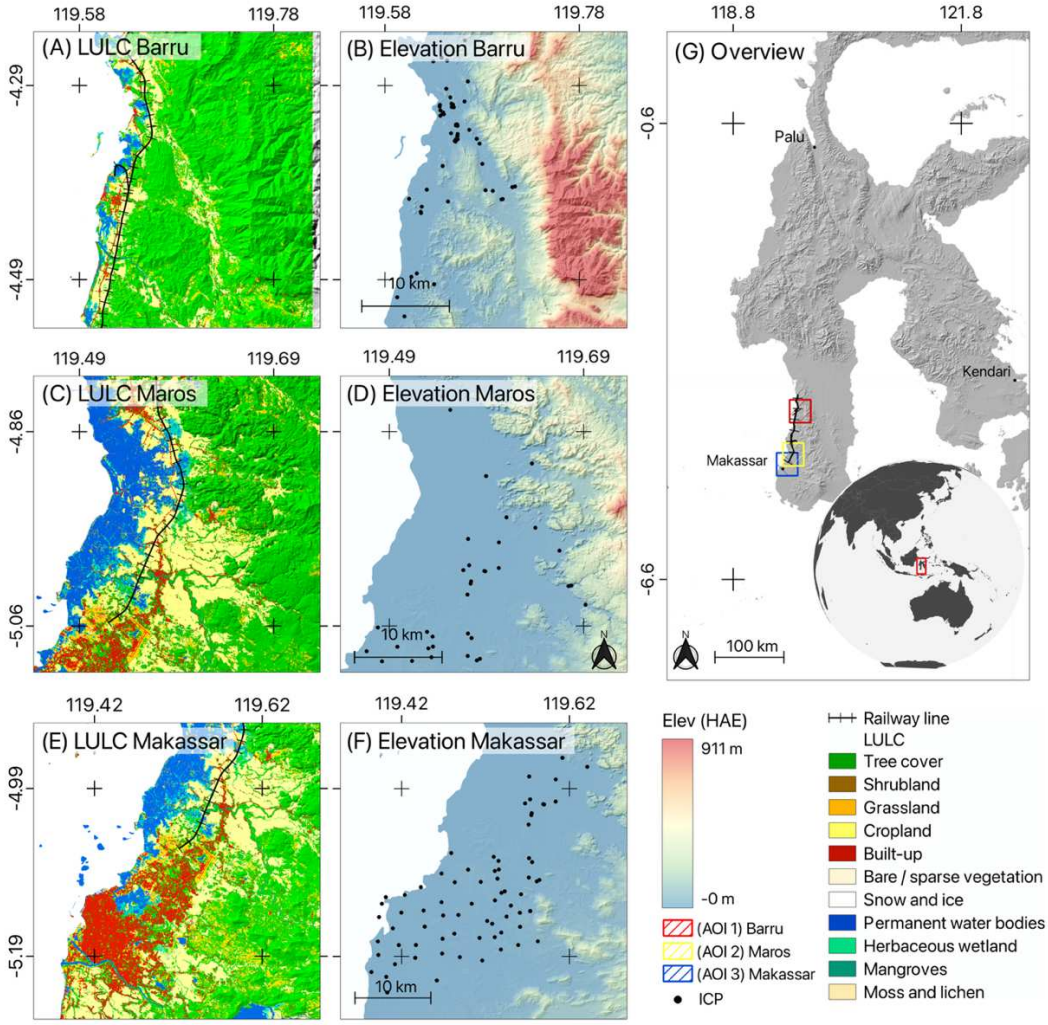

Figure 1. DEM extraction test sites over South Sulawesi Province, (A) LULC Barru, (B) Elevation range Barru, (C) LULC Maros, (D) Elevation range Maros, (E) LULC Makassar, (F) Elevation range Makassar, (G) Overview of South Sulawesi's railway line

In this study, we tested our workflow on three different test sites over South Sulawesi. Each test sites covers 1021 km^2 area. Test site B and C has 41% overlapped region (~417.96 km^2). This gives us a good opportunity to test the geometric and radiometric consistency of the gcp-less DEM extraction method used. The test sites were chosen based on their varying topography and land use/land cover characteristics. We utilize the 2021 10 meter ESA World landcover data (Zanaga et al., 2022) as the land use/land cover reference.

Test site A, located in Barru region represent a rural area dominated with high structural mountain in the eastern part, with relatively flat alluvial plain on the West side. The mountain region is dominated with tree cover while the plain is covered with cropland, built-up, as well as fishpond.

Test site B, located mostly in Maros region, represent a mix of urban and rural region, as it is directly border the province's capital. The Western part is also dominated by mountains, just as test site A. However, these mountains are of the solutional landform, more specifically the Bantimurung-Bulusarawung karst region. The most prominent features for this karst region is its tower karst features. The tower karst exhibit an almost vertical slope that could reach 50 – 100-meter above ground. The flat and fertile alluvial plains can be found on the center parts of the test sites, with larger coverage on the Western part is dominated by aquaculture fishpond. A dense built-up region can be found on the Southwest of the test site.

Test site C, located mostly in Makassar City, represent an urban region with flat alluvial plain for the most region. A gentle denudational hills can be found on the eastern part, albeit not as dominant as the other two test sites. The built-up urban region can be found on the Southwest region with the cropland covers most of the other flat region. The same fishpond on test site B can also be found on the Northwest part of test site C.

b. Datasets

Table 1. Tristereo SPOT-6/7 dataset used. The incidence angle is taken from the "center" pixel and shown in degree

AOI	Dataset ID	Acquisition date	Incidence angle	Remarks
Barru	SPOT7_P_202004170152299	17th April 2020	21.39	Forward
	SPOT7_P_202004170152455	17th April 2020	19.48	Nadir
	SPOT7_P_202004170152575	17th April 2020	18.56	Backward
Maros	SPOT6_P_201809290154426	29th September 2018		Forward
	SPOT6_P_201809290154565	29th September 2018	12.63	Nadir
	SPOT6_P_201809290155321	29th September 2018	8.98	Backward
Makassar	SPOT6_P_201309020158014	02nd September 2013	5.00	Forward
	SPOT6_P_201309020158176	02nd September 2013	2.77	Nadir
	SPOT6_P_201309020158344	02nd September 2013	0.61	Backward

Table 1 shows the SPOT-6/7 tri-stereo datasets used in this study. ALOS World 3D-30m (AW3D30) is a DSM dataset released by Japan Aerospace Exploration Agency (JAXA) with 30 m of spatial resolution, we used the 3.2 version launched in February 2022. It was created by JAXA based on the digital 3D map "ALOS World 3D" (AW3D) (5-meter mesh version). The horizontal accuracy expected to better than 5 m based on its original specification (Nikolakopoulos, 2020; Tadono et al., 2016). The vertical accuracy varied between 3.01 to 11.56 m, generally overestimated dependent on slope, aspect, and landcover (Huang et al., 2024).

DEM Nasional (DEMNAS) is Indonesia specific DEM launched by Indonesian Geospatial Information Agency (BIG) in 2018, it was created from compilation of data from various DEM sources (TerraSAR-X, IFSAR, ALOS PALSAR) and mass point (BIG, 2018). This data was obtained from https://tanahair.indonesia.go.id/portal-web/, available at 0.27 ArcSecond spatial resolution or ~8 m. Recent study discovered that the vertical accuracy of DEMNAS compared to field measurement RMSE and LE90 were 4.968 m and 8.172 m, respectively, worse than official statement of BIG (Susetyo, 2023). In the other hand, DEMNAS present worse error in vertical accuracy in the Karimunjawa archipelago were 6.33 m (RMSE) and 10.45 (LE90) yet still possible to use as reference for producing geomorphological maps with scales of 1:25.000 or smaller (Mutaqin et al., 2023).

Forest And Buildings removed Copernicus DEM (FABDEM) is different type of DEM compared to Global DEM mentioned above. This dataset is generated by remove the bias of building and tree height from COPDEM30 using machine learning approach called random forest regression, then represent the Digital Terrain Model (DTM) (Hawker et al., 2022). It is available at 1 arc second (~30 m) resolution and the reported RMSE is 2.33 m for urban area, 4.96 m for forest area, and 6.66 m for boreal forest area, assessed by LiDAR DTM as reference data. Some study reported that FABDEM showed better performance compared to other DTM in hydrological application including flood hazard mapping or flood modeling related to the land use/land cover variation (Nandam & Patel, 2024). The FABDEM V1-2 data used in this study, released in January 2023 and freely available obtained from https://data.bris.ac.uk/data/dataset

c. Preprocessing

In this study, the tiled based format of SPOT-6/7 tri-stereo, delivered with JP2000 files were merged into a single geotiff file using "`gdal_translate`". In this step, the RPC camera model metadata was written into the same Geotiff file. Next, all three seed DEM's vertical

datum were converted into ellipsoidal vertical datum using the "`dem_geoid`" in AMES Stereo Pipeline (ASP).

d. DEM extraction

The DEM extraction stages were all conducted using NASA's AMES Stereo Pipeline version 3.4.0. The processing were conducted on BRIN's high-performance Computer (BRIN HPC Mahameru 4) with 4 nodes (256 cores), 256GB RAM (Wirahman et al., 2025). The GCP-less DEM extraction workflow is shown in figure 2.

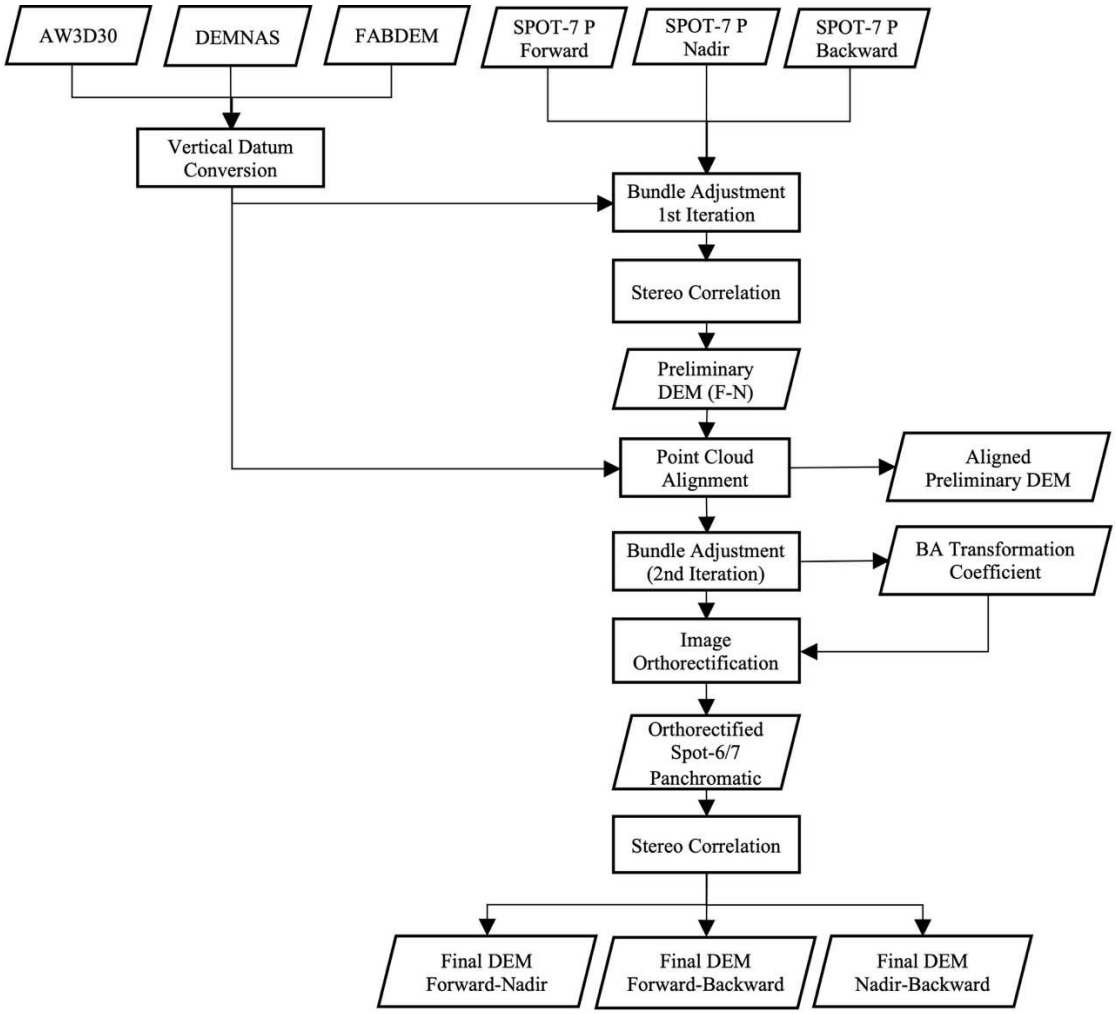

Figure 2. General workflow of the study

The first step is the bundle adjustment (BA). The purpose of this step is to ensure the sensor or camera parameters and position of all three images are adjusted to better align to each other. The bundle adjustment, sometimes also called bundle block adjustment in general utilize the correlation between the 2D image spaces with the 3D object location. We chose the least square algorithm for its faster processing and based on other studies, it gave a good results. For our study we employ the "`parallel_bundle_adjust`" function to maximise the

multiple nodes available in our machine. This step produced a camera orientation and positions variable stored in a text file.

The next step is to perform a preliminary stereo correlation to produce a coarse and smooth initial DEM. To ensure high vertical accuracy, we opted to use the Forward – Backward (FN) stereo pair of the original SPOT-6/7 tri-stereo. Here, we utilize the "`parallel_stereo`" tool and chose the Normalized Cross Correlation (NCC) algorithm for the image correlation algorithm. The detailed parameter used is shown in table 2. We advise to check the ASP's manual for detailed explanation on what each parameters means. This preliminary DEM is generated at a coarser and smoother 20-meter GSD at UTM zone 50 South projection (EPSG:32750). It then co-registered with our seed DEM using ASP's "`pc_align`" tool. The ASP defaulted into the Iterative Closest Point algorithm (Pomerleau et al., 2013; Shean et al., 2016). It is worth mentioning, that other algorithms are available Nuth & Kääb (2011), Fast Global Registration (FGR) (Q. Y. Zhou et al., 2016).

Table 2. Initial DEM stereo correlator parameter using NCC

Parameters	Value
Xcorr – threshold	2
Cost mode	2
Correlation kernel	25
Subpixel kernel	35
Correlation tile size	3200
Correlation memory limit	256000 mb
Subpixel-mode	2

We then performed a second iteration of bundle adjustment using both the first BA output file, and the alignment parameters from the previous "`pc_align`" step. Then, using the transformation data from the second BA, we move onto orthorectifying the original tri-stereo SPOT-6/7 imagery. The refined camera position from the second BA, as well as the initial guess of DEM from the investigated seed DEM, produce orthorectified images at 1.5-meter resolution. This image is comparable to AIRBUS's ORT product.

Table 3. DEM stereo correlator parameter using MGM

Parameters	Value
Xcorr – threshold	2
Cost mode	4
Correlation kernel	7
Subpixel kernel	15
Correlation tile size	3200
Correlation memory limit	256000 mb
Subpixel-mode	2

The second iteration of stereo correlation for DEM extraction then performed iteratively for all three possible pairs (Forward-Nadir, Forward-Backward, and Nadir-Backward). However, for this study we chose the more global matching algorithm (MGM) (Facciolo et al., 2015) for the stereo correlator. Based on previous study, the MGM are able to handle low-texture area and produce smoother surface while maintaining the more complex terrain features (Purinton et al., 2023). Considering most of the rural area are ricefield with relatively smooth surface, we were hoping that MGM would provide good results. Once again utilizing the "`parallel_stereo`" function, the parameters used in this step is shown in table 3. This step produced three point clouds, which then converted into wall-to-wall 6-meter DEM in geotiff format using "`point2dem`". The produced DEM is in ellipsoid vertical datum and EPSG:32750 coordinate reference system. We then re-run the workflow for other study area and other seed DEMs. In total, 27 different scenarios were tested, coming from 3 different test sites, with 3 different seed DEM, and 3 different stereo pair mode (Table 4).

Table 4. 27 different investigated scenario

No	Seed DEM	Region	Pair	No	Seed DEM	Region	Pair	No	Seed DEM	Region	Pair
01	AW3D	Barru	FN	10	AW3D	Maros	FN	19	AW3D	Makassar	FN
02	AW3D	Barru	FB	11	AW3D	Maros	FB	20	AW3D	Makassar	FB
03	AW3D	Barru	NB	12	AW3D	Maros	NB	21	AW3D	Makassar	NB
04	DEMNAS	Barru	FN	13	DEMNAS	Maros	FN	22	DEMNAS	Makassar	FN
05	DEMNAS	Barru	FB	14	DEMNAS	Maros	FB	23	DEMNAS	Makassar	FB
06	DEMNAS	Barru	NB	15	DEMNAS	Maros	NB	24	DEMNAS	Makassar	NB
07	FABDEM	Barru	FN	16	FABDEM	Maros	FN	25	FABDEM	Makassar	FN
08	FABDEM	Barru	FB	17	FABDEM	Maros	FB	26	FABDEM	Makassar	FB
09	FABDEM	Barru	NB	18	FABDEM	Maros	NB	27	FABDEM	Makassar	NB

e. DEM Evaluation

We first check the produced DEMs for visual agreement with the local topography from the reference DEMs. Relief's consistency were also checked. We then performed horizontal shift's calculation using the Nuth & Kaab algorithm (Nuth & Kääb, 2011). As the algorithm calculate the horizontal shifts and iteratively shift's the image to a final coregistered pair, we only use the first iteration horizontal shift's value in x (dx) and y (dy) direction.

We then measured the vertical accuracy using 87 independent control points (ICP) collected during 2021-2022 using GNSS (Trimble Geo7x, Trimble GeoXT, CHC i50, and South S86s). The point's distribution is shown in figure 1. Root mean square error (RMSE), Mean Absolute Error (MAE), and Normalized Median Absolute Deviation (NMAD) were calculate as the quantitative vertical accuracy.

To assess how these initial guess DEMs influence the accuracy on different surface conditions, we then stratified vertical residuals by slope and land cover. The slope were classified into 4 different range (0-5, 5-15, 15-30, >30). Landcover classes was taken from the previously mentioned 2021 ESA WorldCover (Zanaga et al., 2022).

Further analysis were then performed to inspect whether our results shows height-dependent behaviour. Using scatterplot of height residuals we tested the vertical error correlation with the absolute elevation. For each scenario, we fit a robust linear model on the 95% CI where:

$$residual = \propto + \beta \cdot h_{ell}$$

We expect that a near zero slope (β) should indicate a no height-dependent bias.

Results and Discussion

We were able to produce 27 DEMs with 6-meter GSD over 3 seed DEMs on 3 stereo pairs as well as 3 different test sites. Figure 3 provide the visual results of our DEMs. Visual evaluation shows good morphological representation on the hillslope-catchment scales. Large "voids" (No Data value) are visible due to cloud/shadow in the input imagery. Zoomed in view on figure 4 shows that, smaller no-data values occurs on low-texture regions across the 27 DEMs, albeit with different degree of completeness. Visual inspection also shows that no seamline artifact were apparent, and the ridge/valley connectivity is preserved.

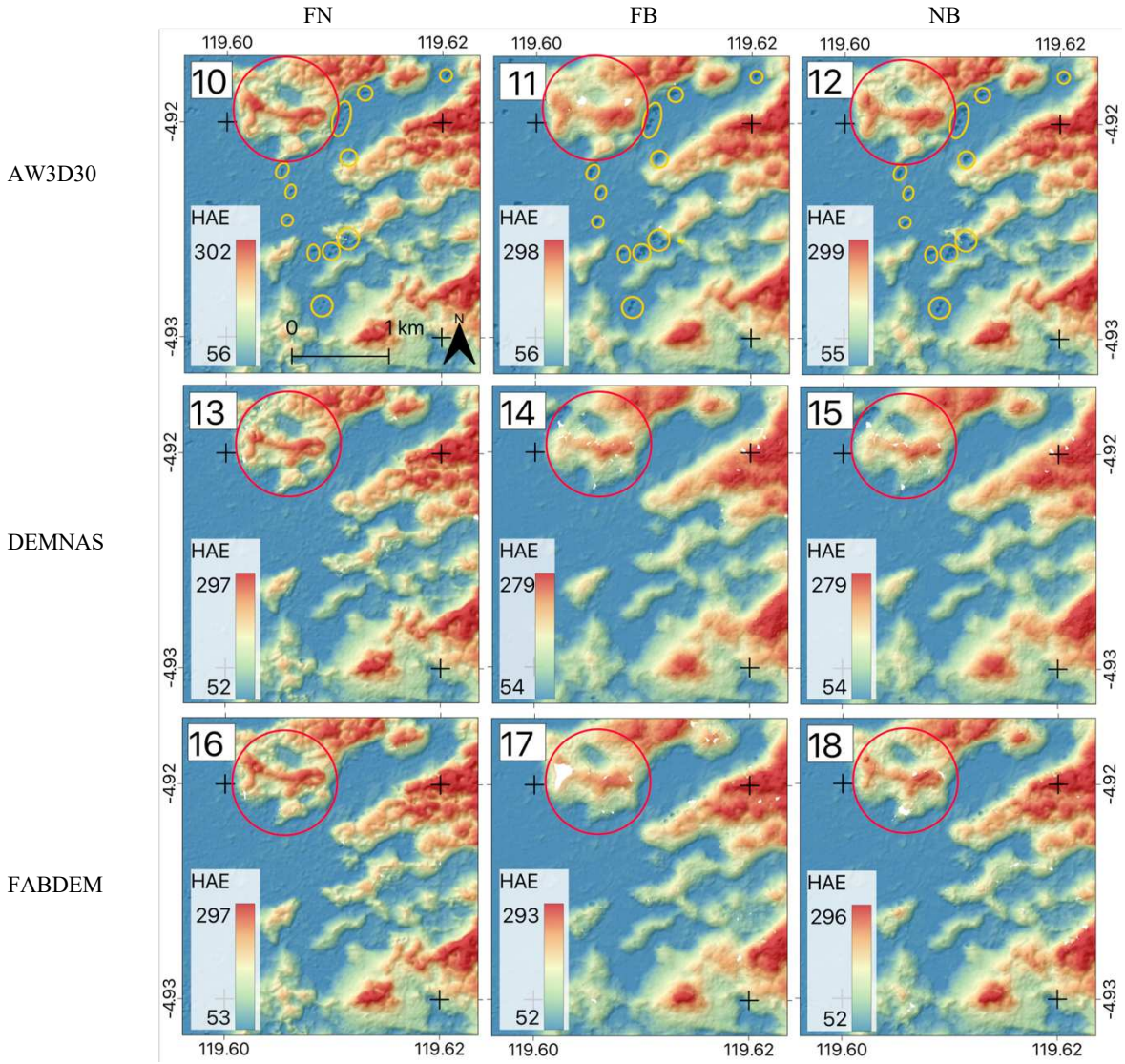

Figure 4. Zoomed in hillshade (AOI 2) where small holes were visible. The number for each image corresponds to the pair numbers shown in table 4. Yellow circles emphasize voids produced by AW3D30. Red circles emphasize different amount of "voids" and topographic details.

Figure 4 showed zoomed in view over AOI 2 (Maros). Here, we found the first evidence of how seed DEM could influence the final product. We found that for AW3D30, small "sinks" are visible to the final DEM (yellow circles). These sinks are originally exist on the AW3D30 version 3.2. Their positions are exactly the same with the final DEM extracted from our approach. We also found that apart from clouds and waterbodies, the produced DEMs are all exhibit small "voids" due to shadows produced by topographic relief and stereo pairs geometry. Red circles in figure 4 emphasize our findings, with an additional detailed differences. These detailed differences, however, is more related to the acquisition geometry, rather than the seed DEM. Forward-Nadir (FN) geometry, consistently produced higher detail compared to the other across three different seed DEMs.

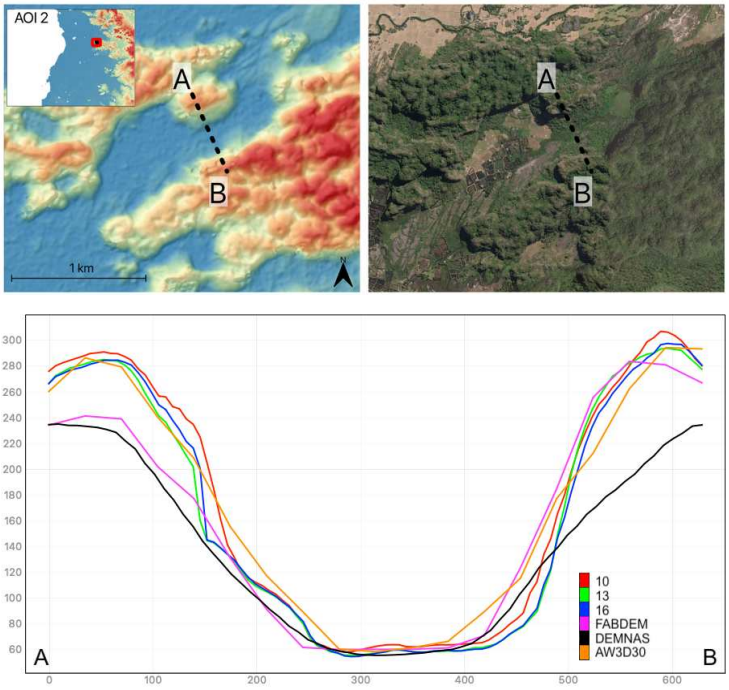

Figure 5. Elevation profile over a subset of AOI 2 (Rammang-rammang village). (A) the produced DEM (pair 13), (B) High-resolution satellite imagery, the elevation profile for pair 10, 13, 16, AW3D30, DEMNAS, and FABDEM.

Figure 5 shows an elevation profile over the same subset in figure 4. The transect line span 620 meter from A to B. Here, we found that for the flat region on the plain all DEMs are mostly agreed to each other. The difference came over the hilltop. Looking at point A, all three produced DEM as well as AW3D30 exhibit high value with recorded elevation just over 260-meter. Both DEMNAS and FABDEM recorded lower value of just under 240-meter on the same starting point. This shows, basically, two different types of DEMs. Our produced DEMs along with AW3D30 is DSM, thus provide higher elevation due to additional surface features. On the other hand, DEMNAS and FABDEM, behave like a true DTM, where the surface feature, which most likely are vegetation, are not included. Looking at the opposite side (B), DEMNAS exhibit lower elevation compared to the other DEMs. DEMNAS also shows a relatively gentle slope compared to the other DEMs shown.

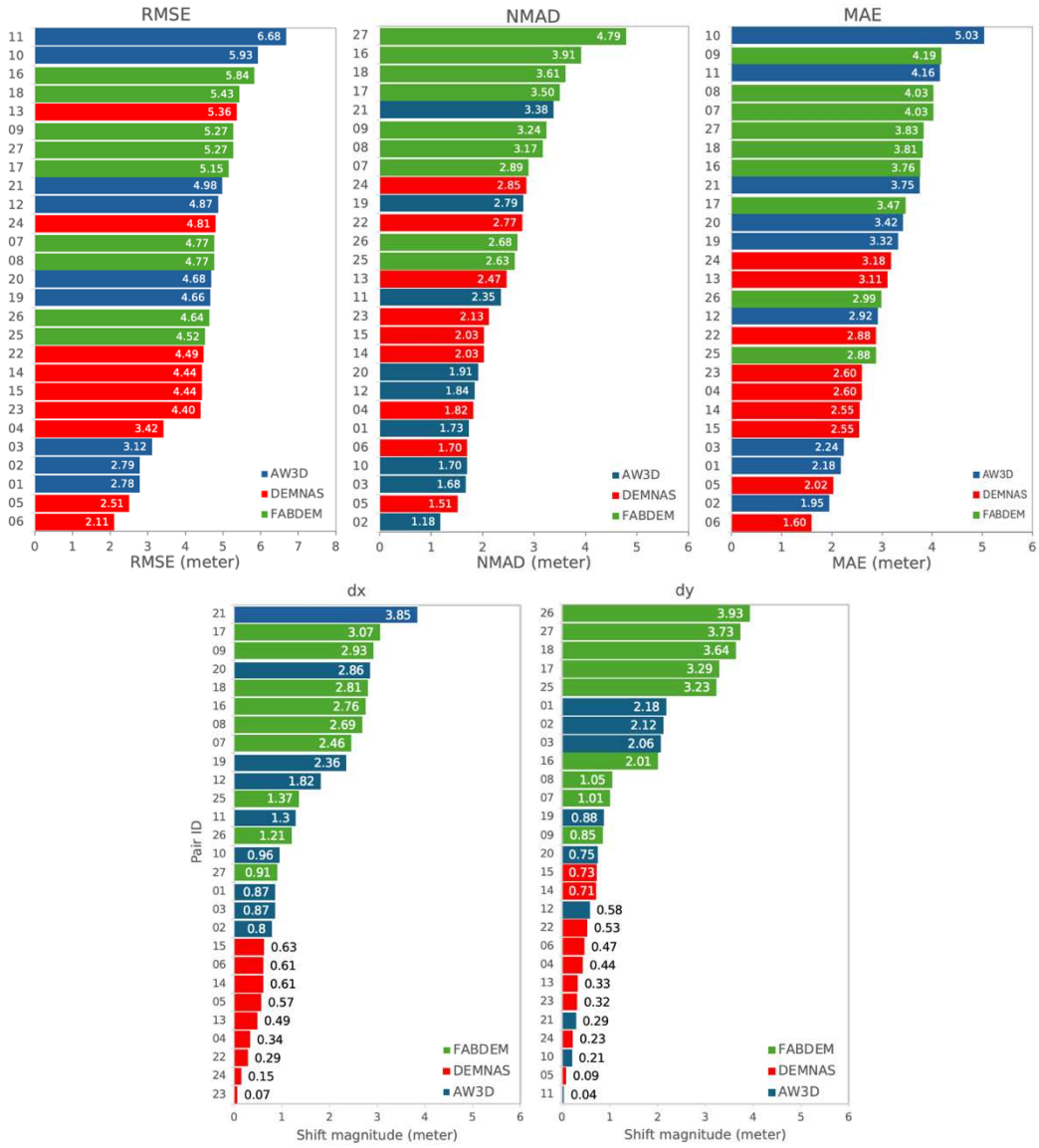

Figure 6. Summary statistics across scenarios on vertical accuracy shown in (a) RMSE, (b) NMAD, (c) MAE, and horizontal shifts in (e) dx, as well as (f) dy direction, sorted in an ascending format.

Figure 6 shows the bar chart of vertical accuracy across all 27 scenarios relative to the 86 GNSS ICPs, with RMSE ranging from 2.11 – 6.68 m, NMAD ranging from 1.18 – 4.79 m, and MAE ranging from 1.60 – 5.03 meter. Looking at each seed DEMs, DEMNAS produced the lowest average of RMSE with 4.00 m, followed by AW3D30 with average RMSE of 4.50. FABDEM came last with average RMSE of 5.07 meter. Based on each test site, DEMNAS consistently produced lowest RMSE for all sites, with an average of 2.68, 4.75, and 4.57 for AOI 1, AOI 2, and AOI 3, respectively.

Furthermore, the horizontal shifts shown in figure 6d and 6e reiterate DEMNAS to have the best results with the tightest alignment. Using DEMNAS, we were able to produce a mean absolute shift of 0.42 m, and 0.43 m for dx, and dy direction, respectively. AW3D30 produced

small, but directionally consistent positive bias of 1.74 m, and 0.88 m on average for *dx*, and *dy* direction, respectively. Lastly, compared to other seed DEM, FABDEM gave the largest shifts with mean absolute error of 2.25 and 2.53 m in negative direction of *dx*, and *dy*, respectively. Considering the 6-m GSD of our DEMs, we deemed that these values are all accurately acceptable.

To this point, we showed that each initial guess DEMs affect both visual and quantitative characteristics of the produced DEM. We then plotted the elevation residuals against different elevation from the GNSS points (Figure 7) with linear fits (95% CI). Here, we found that for there are minimal height-dependent bias for AOI 1 and AOI 2. AOI 3, however, exhibit a height-dependent bias for all three initial seed DEMs.

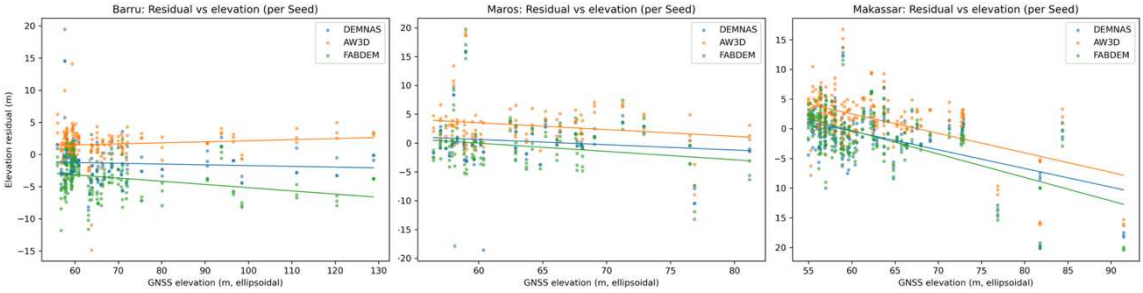

Figure 7. Elevation residuals plotted against GNSS elevation

Our results shows that the initial guess DEMs original trait (DSM/DTM/sink/void) affect the final products. The original sink shown in figure 4 for AW3D30 inherited by its subsequent final DEMs. We originally were not aware of such sink in AOI2, since doline/depression features are expected in karst region. We confirmed this trait by looking at the same phenomena in other test sites that exhibit the same visuals. The main reason for such trait was the use of ICP algorithm on the point cloud adjustment (`pc_align`) phase. ASP utilize the point-to-plane flavor of ICP algorithm during the point cloud alignment phase. We argue that the use of point-to-plane ICP algorithm during point cloud adjustment contributed to the inherited sinks found in our final DEM. Our argument came from the fact that the point-to-plane ICP would consider the sink surface on the AW3D30 as the local surface structure, thus iteratively align our stereo point cloud to minimize the error between two corresponding points (Low, 2004). Fortunately, the latest release of AW3D30 (version 4.1) have corrected these sinks and should eliminates the inherited sinks for our DEMs. Alternatively, other coregistration algorithms is available for point-cloud alignment, as mentioned in method section. How they performed, however, is outside of our current scope.

Large voids on cloud and cloud shadow region found in our study is once again showcase the main limitation of using optical satellite imagery for DEM extraction. This issues have also been acknowledge by previous studies (de Oliveira et al., 2011; Sefercik et al., 2013; Zylshal et al., 2022). While using stereo SAR could mitigate the cloud cover issue (de Oliveira et al., 2011), its limited data availability and considerably lower spatial resolution deemed too big of a gap when compared to our study. We are more drawn to other approach when dealing with these larger gaps. We recommend to use DEM fusion approach (Setiyoko et al., 2019) or the more established DEM void-fill algorithm (Hu et al., 2024; Luedeling et al., 2007). Both of which, is outside of our current scope.

We also acknowledge that our results, have not considered all available global DEM such as CopernicusDEM (Fahrland, 2020), ASTER GDEM (Abrams et al., 2015), MERIT (Yamazaki et al., 2017), TanDEM-X (Zink et al., 2014), SRTM (Farr et al., 2007), and local topographic map. Based on what we found in this study, including these global DEMs could provide better insight on the use of DSM or DTM as the initial seed DEM, as well as its reproducibility worldwide.

While our initial aim is to investigate the initial guess DEMs, we also found that stereo geometry (convergence angle) also plays an important role in DEM quality produced. The recommended practice for base-to-height of 0.3 – 0.7 has been widely accepted (Astrium, 2014), and utilized in our initial request to the image vendor. However, as the user, we seldom have any says on the final delivered product. All datasets we tested were request at minimum of 0.3 to 0.7 b/h. However, with the constraint of cloud cover in our study as well as limited windows of opportunity, the delivered product sometimes only matched the request b/h value on forward-backward geometry. For a high-relief terrain, we recommend to use the forward-backward geometry.

Lastly, as our study investigate tri-stereo acquisition, the use of DEM fusion for all three produced DEMs have not been thoroughly investigated. As the stereo correlation produced point cloud, we could potentially deploy a point cloud fusion between three acquisition geometry and taken the average value of the three pairs (Lu et al., 2016). Other statistical approaches are also available (min, max, median) or even utilizing a weighted average value based on each pair's convergence angle. These options are in our team's plan to investigate in the future.

Conclusions

This study has shown that over 27 produced DEMs, different seed DEMs investigated shows varying degree of influence on DEM vertical and horizontal accuracy. All seed DEMs were able to produce less than a pixel of horizontal shifts, averaging shift's magnitude of 1.32 and 1.46 meters in x and y direction, respectively. Similarly, average vertical accuracy is 3.11, 4.68, and 2.47-meter for MAE, RMSE, and NMAD, respectively. Our study found that the gcp-less DEM produced were all slope dependent as well as geometry and LULC-dependent. Across three different landscapes, DEMNAS produced the most consistent horizontal alignment and lowest vertical errors. AW3D30 also shows a comparably good performance albeit with more variability compared to DEMNAS. FABDEM trails behind the two especially in urban area as well as on the high-relief complex topography. The errors were found to be increased with the slope as well as low texture land use/land cover (waterbody/wetlands/smooth agricultural land).

Our findings suggest that, for Indonesian region, the use of DEMNAS on *Forward-Backward* geometry is preferrable for the gcp-less approach. Other regions where DEMNAS is not available can use the AW3D30 as a reasonable second choice. Lastly, the cloud cover and its subsequent shadows are still an important challenge for optical satellite-derived DEM. Future work should test other available DEMs, especially the one with surface elevation, rather than terrain elevation.

Supplementary

Table 4. Summary statistics on the produced DEM. dx and dy denotes the horizontal shifts with minus "-" value indicates the shift's direction, CA is the convergence angle (degree) for each stereo pair. FN, FB, and NB denotes the Forward-Nadir, Forward-Backward, and Nadir-Backward configuration, respectively. All statistics is shown in meter.

No	Initial_DEM	Region	CA	Pair	dx	dy	MAE	RMSE	NMAD
01	AW3D	Barru	9.23	FN	0.87	2.18	2.18	2.78	1.73
02	AW3D	Barru	16.28	FB	0.80	2.12	1.95	2.79	1.18
03	AW3D	Barru	7.06	NB	0.87	2.06	2.24	3.12	1.68
04	DEMNAS	Barru	9.23	FN	-0.34	0.44	2.60	3.42	1.82
05	DEMNAS	Barru	16.28	FB	-0.57	0.09	2.02	2.51	1.51
06	DEMNAS	Barru	7.06	NB	-0.61	0.47	1.60	2.11	1.70
07	FABDEM	Barru	9.23	FN	-2.46	-1.01	4.03	4.77	2.89
08	FABDEM	Barru	16.28	FB	-2.69	-1.05	4.03	4.77	3.17
09	FABDEM	Barru	7.06	NB	-2.93	-0.85	4.19	5.27	3.24
10	AW3D	Maros	8.9	FN	0.96	0.21	5.03	5.93	1.70
11	AW3D	Maros	30.1	FB	1.30	0.04	4.16	6.68	2.35
12	AW3D	Maros	21.4	NB	1.82	-0.58	2.92	4.87	1.84
13	DEMNAS	Maros	8.9	FN	-0.49	-0.33	3.11	5.36	2.47
14	DEMNAS	Maros	30.1	FB	-0.61	-0.71	2.55	4.44	2.03
15	DEMNAS	Maros	21.4	NB	-0.63	-0.73	2.55	4.44	2.03
16	FABDEM	Maros	8.9	FN	-2.76	-2.01	3.76	5.84	3.91
17	FABDEM	Maros	30.1	FB	-3.07	-3.29	3.47	5.15	3.50
18	FABDEM	Maros	21.4	NB	-2.81	-3.64	3.81	5.43	3.61
19	AW3D	Makassar	10.3	FN	2.36	0.88	3.32	4.66	2.79
20	AW3D	Makassar	20.2	FB	2.86	0.75	3.42	4.68	1.91
21	AW3D	Makassar	10	NB	3.85	0.29	3.75	4.98	3.38
22	DEMNAS	Makassar	10.3	FN	-0.29	0.53	2.88	4.49	2.77
23	DEMNAS	Makassar	20.2	FB	-0.07	0.32	2.60	4.40	2.13
24	DEMNAS	Makassar	10	NB	0.15	0.23	3.18	4.81	2.85
25	FABDEM	Makassar	10.3	FN	-1.37	-3.23	2.88	4.52	2.63
26	FABDEM	Makassar	20.2	FB	-1.21	-3.93	2.99	4.64	2.68
27	FABDEM	Makassar	10	NB	-0.91	-3.73	3.83	5.27	4.79

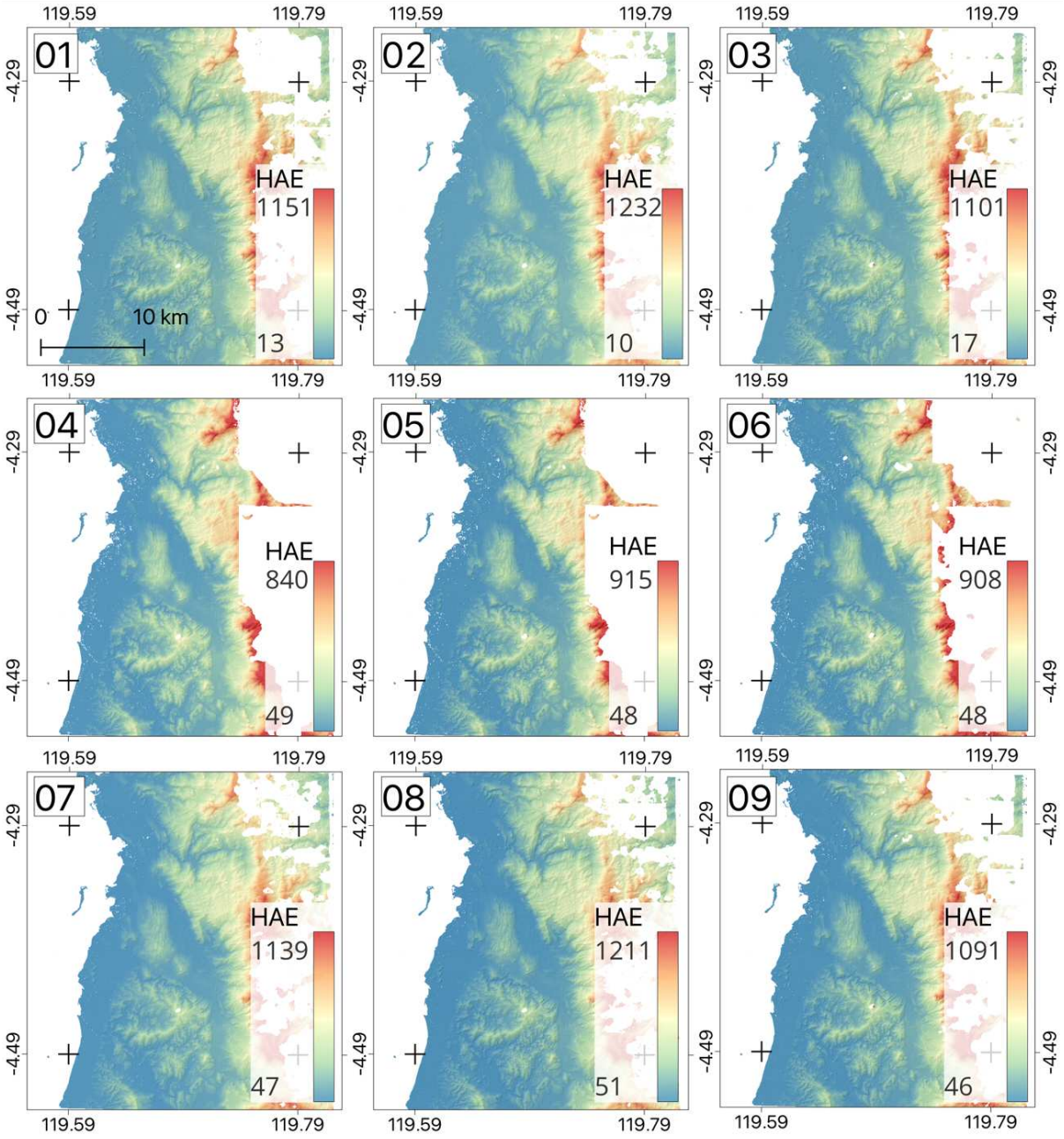

All 27 Produced DEMs shown in its hillshade with the elevation ranges shown in color. The elevation is shown in meters above ellipsoid

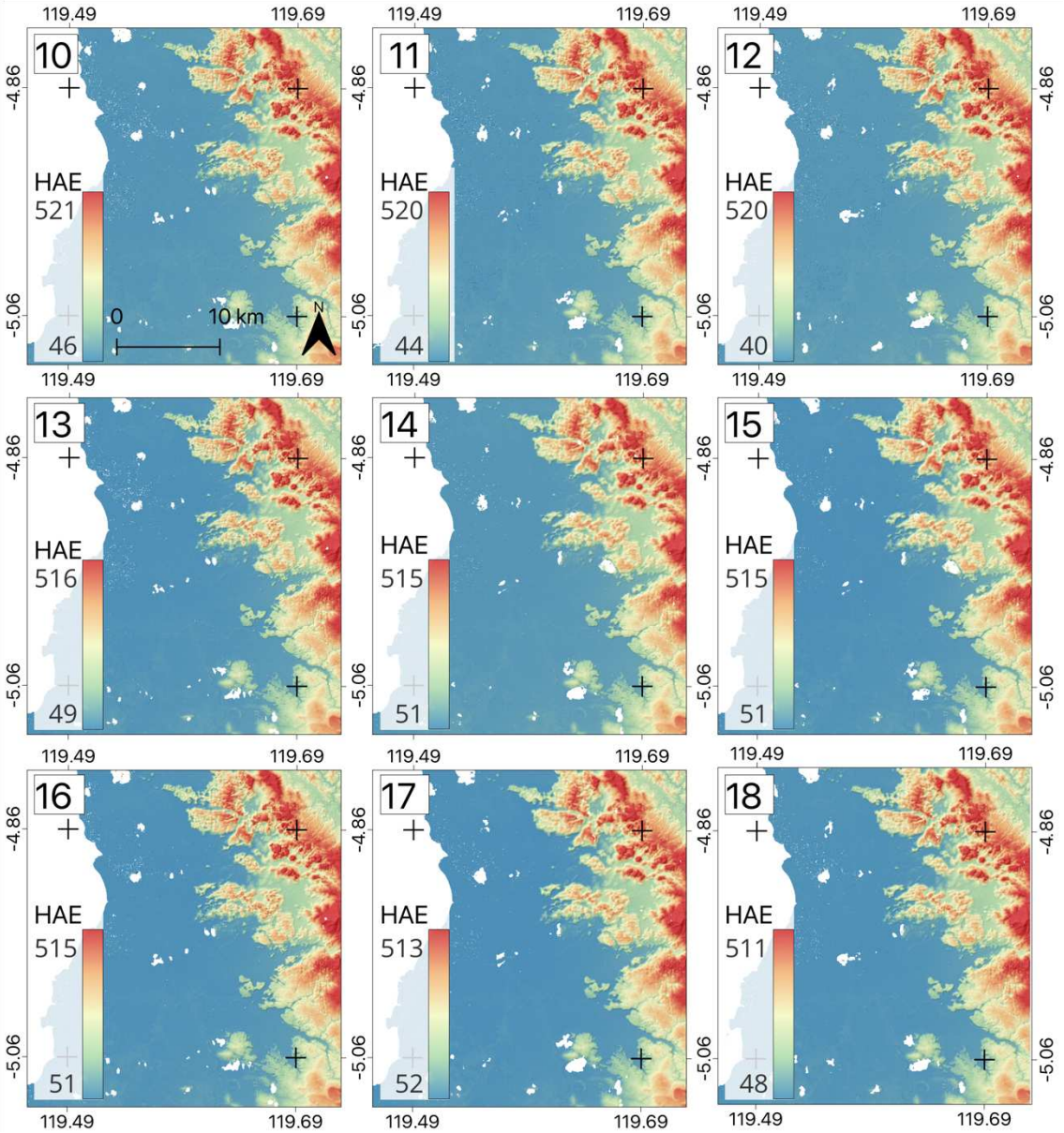
10
HAE
521
46
0
10 km
N
11
HAE
520
44
12
HAE
520
40
13
HAE
516
49
14
HAE
515
51
15
HAE
515
51
16
HAE
515
51
17
HAE
513
52
18
HAE
511
48
119.49
119.69
-4.86
-5.06

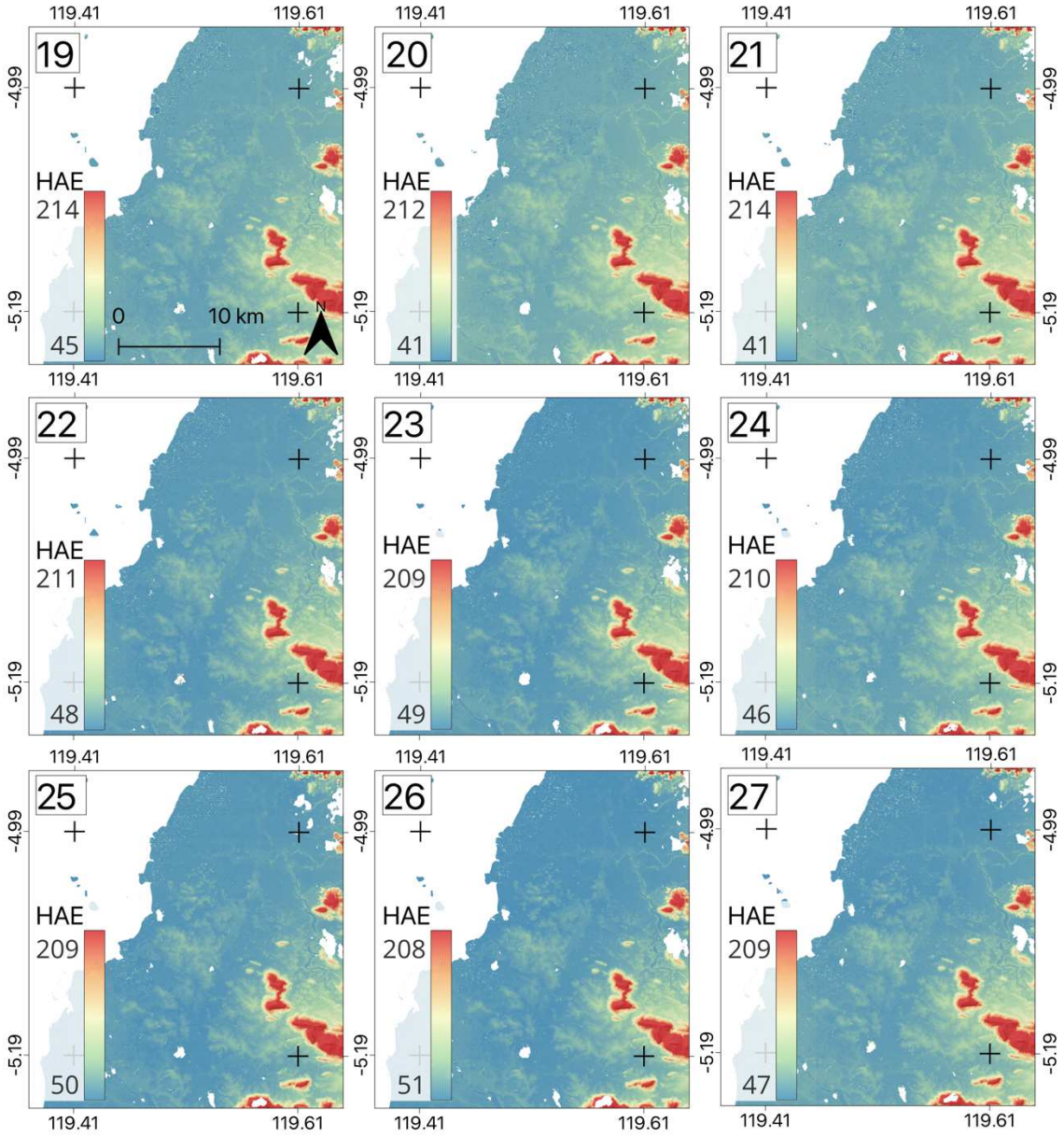

References

Abrams, M., Tsu, H., Hulley, G., Iwao, K., Pieri, D., Cudahy, T., & Kargel, J. (2015). The Advanced Spaceborne Thermal Emission and Reflection Radiometer (ASTER) after fifteen years: Review of global products. *International Journal of Applied Earth Observation and Geoinformation*, *38*, 292–301. https://doi.org/https://doi.org/10.1016/j.jag.2015.01.013

Afsharnia, H., Arefi, H., & Abbasi, M. (2022). Geometric correction of satellite stereo images by DEM matching without ground control points and map projection step: tested on Cartosat-1 images. *Earth Science Informatics*, *15*(2), 1183–1199. https://doi.org/10.1007/s12145-022-00799-3

Astrium. (2014). *SPOT 6/SPOT 7 Technical Sheet*. https://www.l3harris.com/sites/default/files/2023-06/Airbus SPOT 6-7 Technical Data Sheet.pdf

BIG. (2018). *Seamless Digital Elevation Model (DEM) dan Batimetri Nasional*. Badan Informasi Geospasial. https://tanahair.indonesia.go.id/demnas

Cao, H., Tao, P., Li, H., & Shi, J. (2019). Bundle adjustment of satellite images based on an equivalent geometric sensor model with digital elevation model. *ISPRS Journal of Photogrammetry and Remote Sensing*, *156*(August), 169–183. https://doi.org/10.1016/j.isprsjprs.2019.08.011

Carrera-Hernández, J. J. (2021). Not all DEMs are equal: An evaluation of six globally available 30 m resolution DEMs with geodetic benchmarks and LiDAR in Mexico. *Remote Sensing of Environment*, *261*(February). https://doi.org/10.1016/j.rse.2021.112474

Chen, X., Cen, M., Guo, H., Zhang, T., Zhao, C., & Zhang, B. (2018). Chinese satellite photogrammetry without ground control points based on a public DEM using an efficient and robust DEM matching method. *International Journal of Remote Sensing*, *39*(3), 704–726. https://doi.org/10.1080/01431161.2017.1390270

Chen, X., Zhang, B., Cen, M., Guo, H., Zhang, T., & Zhao, C. (2017). SRTM DEM-Aided Mapping Satellite-1 Image Geopositioning Without Ground Control Points. *IEEE Geoscience and Remote Sensing Letters*, *14*(11), 2137–2141. https://doi.org/10.1109/LGRS.2017.2755059

Cooper, P. R., Friedman, D. E., & Wood, S. A. (1987). The automatic generation of digital terrain models from satellite images by stereo. *Acta Astronautica*, *15*(3), 171–180. https://doi.org/10.1016/0094-5765(87)90017-8

de Oliveira, C. G., Paradella, W. R., & da Silva, A. de Q. (2011). Assessment of radargrammetric DSMs from TerraSAR-X Stripmap images in a mountainous relief area of the Amazon region. *ISPRS Journal of Photogrammetry and Remote Sensing*, *66*(1), 67–72. https://doi.org/10.1016/j.isprsjprs.2010.08.008

Facciolo, G., Franchis, C. de, & Meinhardt, E. (2015). MGM: A Significantly More Global Matching for Stereovision. *Proceedings of the British Machine Vision Conference (BMVC)*, *1*, 90.1-90.12. https://doi.org/10.5244/c.29.90

Fahrland, E. (2020). Copernicus dem product handbook (v3. 0). *Airbus Def. Space GmbH Taufkirch. Ger*.

Farr, T. G., Rosen, P. A., Caro, E., Crippen, R., Duren, R., Hensley, S., Kobrick, M., Paller, M., Rodriguez, E., Roth, L., Seal, D., Shaffer, S., Shimada, J., Umland, J., Werner, M., Oskin, M., Burbank, D., & Alsdorf, D. (2007). The Shuttle Radar Topography Mission. *Reviews of Geophysics*, *45*(2). https://doi.org/https://doi.org/10.1029/2005RG000183

Gonçalves, J. A. (2008). Orientation and dem extraction from alos-prism images using the srtm-dem as ground control. *International Archives of the Photogrammetry, Remote Sensing and Spatial Information Sciences - ISPRS Archives*, *37*, 1177 – 1181. https://www.scopus.com/inward/record.uri?eid=2-s2.0-85019345555&partnerID=40&md5=f582a5de47d7ca2f72b9742e5d1a0f18

Hawker, L., Uhe, P., Paulo, L., Sosa, J., Savage, J., Sampson, C., & Neal, J. (2022). A 30 m global map of elevation with forests and buildings removed. *Environmental Research Letters*, *17*(2), 024016. https://doi.org/10.1088/1748-9326/AC4D4F

Hu, Z., Gui, R., Hu, J., Fu, H., Yuan, Y., Jiang, K., & Liu, L. (2024). InSAR Digital Elevation Model Void-Filling Method Based on Incorporating Elevation Outlier Detection. *Remote Sensing*, *16*(8). https://doi.org/10.3390/rs16081452

Huang, J., Yang, Y., Yu, Y., & Zhang, Y. (2024). Vertical accuracy of open-source remote sensing data (AW3D30, TanDEM-X, ATLAS) for understory terrain estimation. *Geocarto International*, *39*(1). https://doi.org/10.1080/10106049.2024.2356855

Julzarika, A., & Harintaka. (2019). Indonesian DEMNAS: DSM or DTM? *AGERS 2019 - 2nd IEEE Asia-Pacific Conference on Geoscience, Electronics and Remote Sensing Technology*, 31–36. https://doi.org/10.1109/AGERS48446.2019.9034351

Lee, H., & Hahn, M. (2024). ICESat-2 Data Application for DEM Bias Compensation Based

on Point-to-Surface Matching. *IEEE Transactions on Geoscience and Remote Sensing*, *62*, 1–11. https://doi.org/10.1109/TGRS.2024.3396292

Low, K.-L. (2004). Linear least-squares optimization for point-to-plane icp surface registration. *Chapel Hill, University of North Carolina*, *4*(10), 1–3. https://www.comp.nus.edu.sg/~lowkl/publications/lowk_point-to-plane_icp_techrep.pdf

Lu, S., Huang, S., Pan, Z., Deng, H., Stanley, D., & Xin, Y. (2016). HIGH PERFORMANCE COMPUTING for DSM EXTRACTION from ZY-3 TRI-STEREO IMAGERY. *ISPRS Annals of the Photogrammetry, Remote Sensing and Spatial Information Sciences*, *3*(July), 113–120. https://doi.org/10.5194/isprs-annals-III-1-113-2016

Luedeling, E., Siebert, S., & Buerkert, A. (2007). Filling the voids in the SRTM elevation model - A TIN-based delta surface approach. *ISPRS Journal of Photogrammetry and Remote Sensing*, *62*(4), 283–294. https://doi.org/10.1016/j.isprsjprs.2007.05.004

Mutaqin, B. W., Isnain, M. N., Marfai, M. A., Fatchurohman, H., Quesada-Román, A., & Khakhim, N. (2023). Assessing the accuracy of open-source digital elevation models for the geomorphological analysis of very small islands of Indonesia. *Applied Geomatics*, *15*(4), 957–974. https://doi.org/10.1007/s12518-023-00533-8

Nandam, V., & Patel, P. L. (2024). On the role of digital terrain topography and land use dynamics in flood hazard assessment of urban floodplain. *Natural Hazards*, *120*(13), 11877–11902. https://doi.org/10.1007/s11069-024-06664-4

Neigh, C. S. R., Masek, J. G., Bourget, P., Cook, B., Huang, C., Rishmawi, K., & Zhao, F. (2014). Deciphering the precision of stereo IKONOS canopy height Models for US forests with G-LiHT airborne LiDAR. *Remote Sensing*, *6*(3), 1762–1782. https://doi.org/10.3390/rs6031762

Nikolakopoulos, K. G. (2020). Accuracy assessment of ALOS AW3D30 DSM and comparison to ALOS PRISM DSM created with classical photogrammetric techniques. *European Journal of Remote Sensing*, *53*(sup2), 39–52. https://doi.org/10.1080/22797254.2020.1774424

Nuth, C., & Kääb. (2011). Co-registration and bias corrections of satellite elevation data sets for quantifying glacier thickness change. *Cryosphere*, *5*(1), 271–290. https://doi.org/10.5194/tc-5-271-2011

Pomerleau, F., Colas, F., Siegwart, R., & Magnenat, S. (2013). Comparing ICP variants on real-world data sets: Open-source library and experimental protocol. *Autonomous Robots*, *34*(3), 133–148. https://doi.org/10.1007/s10514-013-9327-2

Purinton, B., Mueting, A., & Bookhagen, B. (2023). Image Texture as Quality Indicator for Optical DEM Generation: Geomorphic Applications in the Arid Central Andes. *Remote Sensing*, *15*(1), 85. https://doi.org/10.3390/rs15010085

Sefercik, U. G., Alkan, M., Buyuksalih, G., & Jacobsen, K. (2013). Generation and Validation of High-Resolution DEMs from Worldview-2 Stereo Data. *Photogrammetric Record*, *28*(144), 362–374. https://doi.org/10.1111/phor.12038

Setiyoko, A., Arymurthy, A. M., & Basaruddin, T. (2019). DEM fusion concept based on the LS-SVM cokriging method. *International Journal of Image and Data Fusion*, *10*(4), 244–262. https://doi.org/10.1080/19479832.2019.1664647

Shean, D. E., Alexandrov, O., Moratto, Z. M., Smith, B. E., Joughin, I. R., Porter, C., & Morin, P. (2016). An automated, open-source pipeline for mass production of digital elevation models (DEMs) from very-high-resolution commercial stereo satellite imagery. *ISPRS Journal of Photogrammetry and Remote Sensing*, *116*(206), 101–117. https://doi.org/10.1016/j.isprsjprs.2016.03.012

Susetyo, D. B. (2023). Vertical Accuracy Assessment of Various Open-Source Dem Data: Demnas, Srtm-1, and Aster Gdem. *Geodesy and Cartography (Vilnius)*, *49*(4), 209–215. https://doi.org/10.3846/gac.2023.18168

Swann, R., Kauffmann, D., & Sharpe, B. (1988). Results of automated digital elevation model generation from SPOT satellite data. *International Archives of Photogrammetry and Remote Sensing*, *27*(B2), 434–440.

Tadono, T., Nagai, H., Ishida, H., Oda, F., Naito, S., Minakawa, K., & Iwamoto, H. (2016). Generation of the 30 M-MESH global digital surface model by alos prism. *International Archives of the Photogrammetry, Remote Sensing and Spatial Information Sciences - ISPRS Archives*, *41*(July), 157–162. https://doi.org/10.5194/isprsarchives-XLI-B4-157-2016

Wirahman, T., Latifah, A. L., Muttaqien, F. H., Swardiana, I. W. A., Arisal, A., Iryanto, S. B., & Sadikin, R. (2025). Performance Evaluation of NAS Parallel and High-Performance Conjugate Gradient Benchmarks in Mahameru. *Jurnal Online Informatika*, *10*(2), 248–259. https://doi.org/10.15575/join.v10i2.1557

Yamazaki, D., Ikeshima, D., Neal, J. C., O'Loughlin, F., Sampson, C. C., Kanae, S., & Bates, P. D. (2017). MERIT DEM: A new high-accuracy global digital elevation model and its merit to global hydrodynamic modeling. *AGU Fall Meeting Abstracts*, *2017*, H12C--04.

Zanaga, D., Van De Kerchove, R., Daems, D., De Keersmaecker, W., Brockmann, C., Kirches, G., Wevers, J., Cartus, O., Santoro, M., Fritz, S., Lesiv, M., Herold, M., Tsendbazar, N.-E., Xu, P., Ramoino, F., & Arino, O. (2022). *ESA WorldCover 10 m 2021 v200*. Zenodo. https://doi.org/10.5281/zenodo.7254221

Zheng, M., & Zhang, Y. (2016). DEM-Aided Bundle Adjustment With Multisource Satellite Imagery : ZY-3 and GF-1 in Large Areas. *IEEE Geoscience and Remote Sensing Letters*, *13*(6), 880–884. https://doi.org/10.1109/LGRS.2016.2551739

Zhou, P., Tang, X., Guo, L., Wang, X., & Fan, W. (2018). DEM generation using Ziyuan-3 mapping satellite imagery without ground control points. *International Journal of Remote Sensing*, *39*(19), 6213–6233. https://doi.org/10.1080/01431161.2018.1456702

Zhou, Q. Y., Park, J., & Koltun, V. (2016). Fast global registration. *Lecture Notes in Computer Science (Including Subseries Lecture Notes in Artificial Intelligence and Lecture Notes in Bioinformatics)*, *9906 LNCS*, 766–782. https://doi.org/10.1007/978-3-319-46475-6

Zink, M., Bachmann, M., Bräutigam, B., Fritz, T., Hajnsek, I., Krieger, G., Moreira, A., & Wessel, B. (2014). TanDEM-X: The new global DEM takes shape. *IEEE Geoscience and Remote Sensing Magazine*, *2*(2), 8–23. https://doi.org/10.1109/MGRS.2014.2318895

Zylshal, Z., Bayanuddin, A. A., Sartika, S., Pratiwi J, I., Musyarofah, M., & Khomarudin, M. R. (2024). Iterative Bundle Adjustment Without Ground Control Points on SPOT-7 Stereogrammetry and Its Effect on DEM Geometric Accuracy. In A. Blanco, A. B. Rimba, C. M. Roelfsema, & S. Arjasakusuma (Eds.), *Proc. SPIE 12977, Eighth Geoinformation Science Symposium 2023: Geoinformation Science for Sustainable Planet* (Issue January). SPIE. https://doi.org/10.1117/12.3009209

Zylshal, Z., Sartika, S., Bayanuddin, A. A., Munawar, S. T. A., Hestrio, Y. F., Hidayat, S., Pratiwi, I., Setiyoko, A., & Setiawan, W. (2022). Stereo vs. tri-stereo: Preliminary results on Anthropogenic-induced landform change detection using satellite derived remote sensing data. *2022 IEEE International Conference on Aerospace Electronics and Remote Sensing Technology, ICARES 2022 - Proceedings*, 1–7. https://doi.org/10.1109/ICARES56907.2022.9993523